Experimental observation of the dependence of Autler-Townes splitting on the probe and coupling laser wave-number ratio in Doppler-broadened open molecular cascade systems

A. Lazoudis,[1] E. H. Ahmed,[1] L. Li,[2] T. Kirova,[1] P. Qi,[1] A. Hansson,[3] J. Magnes,[4] and A. M. Lyyra[1]
[1]*Department of Physics, Temple University, Philadelphia, Pennsylvania 19122, USA*
[2]*Department of Physics and Key Laboratory of Atomic and Molecular Nanosciences, Tsinghua University, Beijing 100084, China*
[3]*Physics Department, Stockholm University, Alba Nova, SE-10691 Stockholm, Sweden*
[4]*Physics and Astronomy Department, Vassar College, Poughkeepsie, New York 12604, USA*
(Received 8 July 2008; published 7 October 2008)

We have investigated the effects of inhomogeneous Doppler line broadening on the Autler-Townes (AT) splitting in a three-level open molecular cascade system. For moderate Rabi frequencies in the range of 300–600 MHz, the fluorescence line shape from the uppermost level $|3\rangle$ in this system depends strongly on the wave-number ratio of the two laser fields. However, the fluorescence spectrum of the intermediate level $|2\rangle$ appears as expected. We provide a description of the conditions for optimally resolved AT splitting in terms of the ratio of the probe and coupling laser wave numbers, and the laser propagation geometry based on our theoretical analysis of the Doppler integral. The low threshold Rabi frequency region for Autler-Townes splitting is important for high-resolution Autler-Townes spectroscopy since the laser E-field amplitudes are modest in continuous-wave laser experiments.

DOI: 10.1103/PhysRevA.78.043405 PACS number(s): 33.40.+f, 42.50.Hz

I. INTRODUCTION

Studies of coherence and quantum interference effects [1] such as Autler-Townes (AT) splitting and electromagnetically induced transparency (EIT) in atomic and molecular systems have attracted a great deal of attention because they yield a number of important potential applications, including the production of slow light [2], lasing without inversion [3], pulse-matching effects [4], and control of the index of refraction [5]. EIT was demonstrated for the first time by Boller *et al.* [6] in an atomic Λ-type strontium system. It renders an otherwise optically thick medium transparent to a weak laser field. Most of the previous theoretical and experimental work on EIT and AT was based on various three-level closed atomic systems with different energy level configurations using both pulsed and continuous wave (cw) lasers [7–13]. It is generally expected that high coupling field intensities are required for observation of AT splitting and EIT to overcome the inhomogeneous Doppler broadening. Nevertheless, it has been shown that with proper selection of experimental parameters and beam geometry, it is possible to overcome this difficulty and to demonstrate these effects in both atomic [8] and molecular systems [14–17] with coupling field Rabi frequencies produced by commercially available cw lasers.

Previously, we emphasized that the AT effect can be used to measure directly the absolute value of the molecular transition dipole moment [14,15] and its internuclear distance dependence [18] as well as to facilitate control of molecular angular momentum alignment [16]. In this paper, we investigate experimentally the unexpected role of inhomogeneous Doppler line broadening on the experimental observation of AT splitting and EIT in a three-level open molecular cascade system. These anomalies include the observation of a dramatic change in the fluorescence line shape observed from the uppermost level of the cascade excitation scheme, while at the same time the fluorescence line shape observed from the intermediate level is marginally affected. Using our earlier theoretical analysis of the three-level Doppler-broadened open molecular cascade system [19], we discuss the experimental results and provide a description of the optimal experimental conditions for the observation of AT splitting in terms of the ratio of the probe and coupling laser wave numbers as well as their relative propagation direction.

II. EXPERIMENT

The experimental details have been described previously in Refs. [14,16]. Schematic illustrations of the excitation schemes used in the experiments are displayed in Fig. 1, with a list of the relevant experimental parameters given in Table I. The two schemes illustrated in Fig. 1 have different values for the ratio, $x=k_1/k_2$, of the probe laser wave number k_1 to that of the coupling laser k_2, with the ratio having positive values for copropagating and negative for counterpropagat-

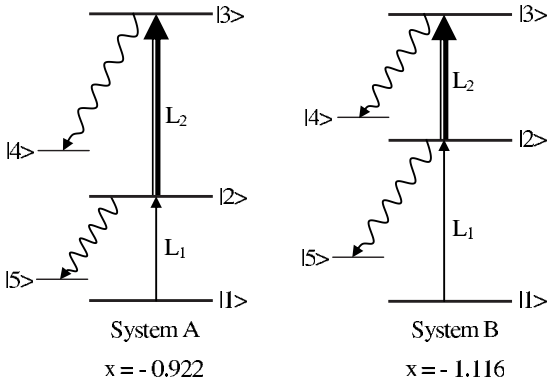

FIG. 1. The Na_2 cascade excitation scheme for two different probe laser–coupling laser wave-number ratios $x=k_1/k_2$. In system A, $-1<x<0$ and in system B, $x<-1$. Intermediate level $|2\rangle$ belongs to the Na_2 $A\ ^1\Sigma_u^+$ state and the uppermost level belongs to the $2\ ^1\Pi_g$ state in system A and to the $4\ ^1\Sigma_g^+$ state in system B, respectively.

TABLE I. List of the experimental parameters for systems A and B. With k we denote the laser wave number, w is the radius of the laser beam defined as $1/e^2$ of the peak power at the center of the beam, P is the total power of the laser beam, μ is the transition dipole moment matrix element, and Ω is the Rabi frequency.

		Transition						
		Energy levels	k (cm^{-1})	w_e (μm)	P (mW)	μ (Debye)	$\Omega/2\pi$ (MHz)
System A	$\|1\rangle \rightarrow \|2\rangle$, L_1	$X\ ^1\Sigma_g^+(0,19) \rightarrow A\ ^1\Sigma_u^+(0,20)$	14647.55	145	1.0	0.25	6
	$\|2\rangle \rightarrow \|3\rangle$, L_2	$A\ ^1\Sigma_u^+(0,20) \rightarrow 2\ ^1\Pi_g(0,19)$	15888.06	340	130	4.16	485
System B	$\|1\rangle \rightarrow \|2\rangle$, L_1	$X\ ^1\Sigma_g^+(1,19) \rightarrow A\ ^1\Sigma_u^+(3,18)$	14828.63	165	0.35	2.88	36
	$\|2\rangle \rightarrow \|3\rangle$, L_2	$A\ ^1\Sigma_u^+(3,18) \rightarrow 4\ ^1\Sigma_g^+(0,17)$	13284.55	550	270	5.06	530

ing beams. For system A, we have chosen the ratio to be in the interval $-1<x<0$ ($x=-0.922$), while for system B we have chosen it to be $x<-1$ ($x=-1.116$). For the two systems we have chosen the particular transitions fulfilling the above criteria for the value of x in such a way that the coupling transition has as large as possible transition dipole moment in order to maximize the Rabi frequency of the coupling field given the available laser sources: narrowband frequency stabilized dye and titanium sapphire lasers (Coherent Autoscan 699-29 and 899-29). The experiments were performed with sodium dimer molecules prepared in a heat pipe loaded with sodium metal and argon as buffer gas. The working temperature of the heat pipe was about 625 K and the pressure of the buffer gas was 200 m Torr at room temperature. The probe laser (L_1) excites the Na_2 molecules from a thermally populated rovibrational level $|1\rangle$ of the $X\ ^1\Sigma_g^+$ electronic ground state to the intermediate level $|2\rangle$ belonging to the Na_2 $A\ ^1\Sigma_u^+$ state, which is coupled by the coupling laser (L_2) to the uppermost level $|3\rangle$ belonging to the $2\ ^1\Pi_g$ state in system A, and to the $4\ ^1\Sigma_g^+$ state in system B. With the coupling laser tuned to resonance, we scanned the probe laser and detected fluorescence originating from level $|2\rangle$ and level $|3\rangle$ by monitoring a specific rovibrational fluorescence channel with a Spex 1404 double monochromator acting as a narrowband filter.

III. RESULTS AND DISCUSSION

In both systems, the fluorescence from the intermediate level $|2\rangle$ displayed the EIT pattern expected in an open molecular system [14] as illustrated in Figs. 2(a) and 2(b). However, the AT splitting, which is generally present in the fluorescence spectrum from level $|3\rangle$ for a sufficiently large coupling field Rabi frequency, is quite sensitive to the wave-number ratio $x=k_1/k_2$. For counterpropagating laser beams when $-1<x<0$ as in system A, we observed a clear AT splitting, as shown in Fig. 3(a), whereas in system B with $x<-1$, we did not observe any AT splitting at all [see Fig. 3(b)].

For simulating the experimental spectra from Figs. 2 and 3, we use the density matrix formalism for the excitation schemes given in Fig. 1. The intensity of the excitation spectra from the intermediate $|2\rangle$ or upper $|3\rangle$ levels can be written as

$$I_k = \sum_M \int_{-\infty}^{+\infty} \rho_{kk}^M(v_z) N(v_z) dv_z, \quad k=2,3, \tag{1}$$

where the summation over the index M takes into account the presence of magnetic sublevel substructure in the rovi-

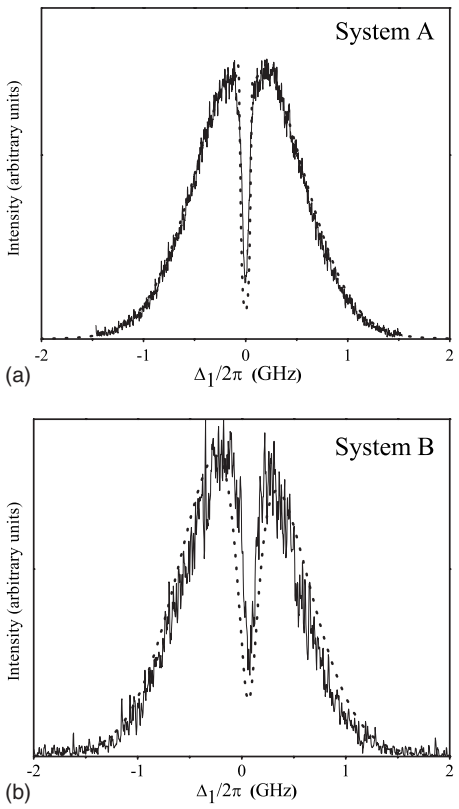

FIG. 2. Observation of EIT by fluorescence detection from the intermediate level as a function of the probe laser detuning for counterpropagating beams for systems A and B. The Doppler width is about 1.15 GHz corresponding to 625 K sample temperature. The fluorescence channels used for recording the spectra are $A\ ^1\Sigma_u^+(0,20) \rightarrow X\ ^1\Sigma_g^+(3,21)$ and $A\ ^1\Sigma_u^+(3,18) \rightarrow X\ ^1\Sigma_g^+(2,19)$ for systems A and B, respectively. In the scan for system A, the coupling laser is exactly on resonance $\Delta_2=0$, while in the scan for system B, it was slightly off resonance with $\Delta_2=60$ MHz. The experimental scan and the simulation are shown by solid and dashed lines, respectively.

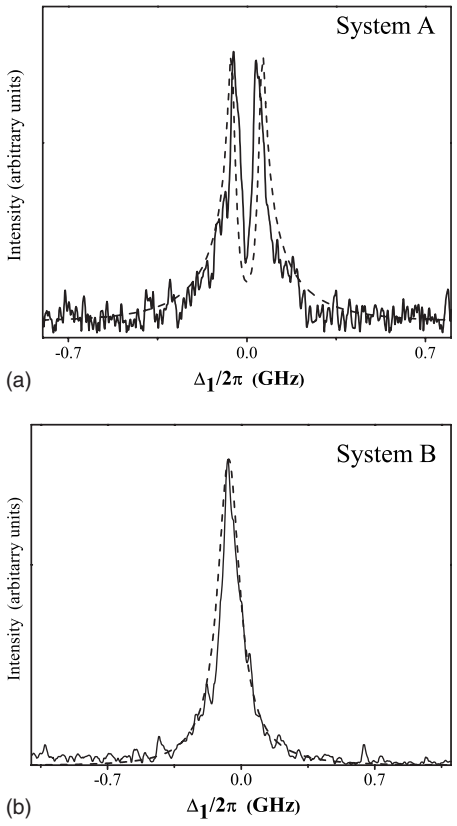

FIG. 3. Fluorescence signal from level $|3\rangle$ as a function of the detuning of the probe laser Δ_1. The fluorescence channels used for recording the spectra are $2\,^1\Pi_g(0,19)\rightarrow A\,^1\Sigma_u^+(0,18)$ and $4\,^1\Sigma_g^+(0,17)\rightarrow A\,^1\Sigma_u^+(1,16)$ for systems A and B, respectively. For system A with $k_1/k_2=-0.922$, we observe well-resolved AT splitting, while for system B with $k_1/k_2=-1.116$, the AT splitting is not resolved despite the similar coupling Rabi frequencies for both cases. In the scan for system A, the coupling laser is exactly on resonance $\Delta_2=0$, while in the scan for system B, it was slightly off resonance with $\Delta_2=60$ MHz. The experimental scan and the simulation are shown by solid and dashed lines, respectively.

brational levels of the molecules. $\rho_{kk}^M(v_z)$ are the diagonal density matrix elements representing the population in the kth level. They are calculated using the exact analytical solution of the steady-state density matrix equation of motion for the molecular cascade excitation scheme given in Ref. [19]. For the velocity distribution $N(v_z)$, we use the Maxwell-Boltzmann distribution

$$N(v_z)=\frac{N_0}{u\sqrt{\pi}}\exp\left(-\frac{v_z^2}{u^2}\right). \tag{2}$$

v_z is the z component of the translational velocity of the molecules.

Our Rabi frequencies ($\Omega/2\pi=\mu E/\hbar$) were 6 and 485 MHz for the probe and coupling fields for system A, and 36 and 530 MHz for the probe and coupling fields for system B. The E-field amplitude in the interaction region was experimentally determined from measurements of the laser beam spotsize w and the total laser power P. The transition dipole moment matrix elements μ were calculated from *ab initio* electronic transition dipole moment functions $\mu_e(R)$ [20] and the potential curves of the relevant electronic states [21–24] using the computer program LEVEL [25]. Since the transition dipole moments used for calculation of the Rabi frequencies for the simulations are based on theoretical *ab initio* $\mu_e(R)$ calculations, the simulations in Figs. 2 and 3 may not be optimal in the absence of more accurate experimental $\mu_e(R)$ functions. The values of these parameters for both systems are given in Table I. The simulations also require knowledge of the lifetimes of the levels participating in the excitation scheme. The lifetime of level $|2\rangle$ in systems A and B is 12.2 ns [26]. Since there are no experimentally measured values for the lifetime of level $|3\rangle$ for systems A and B available, we have calculated them according to the general procedure outlined in [27] and using the computer program LEVEL 7.7 by Le Roy [25] for calculating the decay rates. The program input requires the potential energy curves of the relevant electronic states [21–23,28–30] and the electronic transition dipole moment functions between them [20]. We have obtained 21.0 and 12.7 ns for the lifetime of level $|3\rangle$ of system A and B, respectively. We have calculated the transit relaxation rate w_t according to Ref. [31].

Our results showed that the presence (or absence) of a splitting in the fluorescence spectra of the upper level $|3\rangle$ depends in a sensitive way on the wave-number ratio of the probe and coupling lasers. This nonintuitive behavior in the fluorescence line shape from level $|3\rangle$ in a Doppler-broadened sample can be explained by applying the theoretical analysis given in Ref. [19] to our systems. The minimum value of Ω_2 that is required in order for AT splitting to be observed is denoted by Ω_2^T. From the condition for change in the curvature of $I_3(\Delta_1)$ at zero detuning of the probe laser

$$\left.\frac{d^2I_3(\Delta_1)}{d\Delta_1^2}\right|_{\Delta_1=0}=0, \tag{3}$$

one can calculate the threshold value Ω_2^T. Results obtained for Ω_2^T as a function of $1/x$ from Eq. (3) are given in Fig. 4. The dashed line represents a calculation using parameters for system A and the solid line is with parameters for system B. The difference between the two curves for Ω_2^T arises mainly from the sixfold different probe Rabi frequencies between the two experiments—system A, $\Omega_1/2\pi=6$ MHz and system B, $\Omega_1/2\pi=36$ MHz. We have illustrated the dependence of Ω_2^T on Ω_1 in Fig. 5, where the parameters used in the calculations are for system B. The figure shows that there is a strong dependence of Ω_2^T on the probe laser Rabi frequency Ω_1, and Ω_2^T reaches a minimum when $\Omega_1\rightarrow 0$ as expected, excluding the case $\Omega_1=0$ when there is no population in levels $|2\rangle$ and $|3\rangle$. Thus, for experimental observation of the AT splitting, it is preferable to work with as low power on the probe laser as possible while still maintaining a reasonable signal-to-noise ratio. As the graph shows, Ω_2^T is very small in the counterpropagating case for $-1<x<0$ $(-\infty<1/x<-1)$ and does not depend on the Doppler linewidth [19]. In the case of $x<-1$ $(-1<1/x<0)$, Ω_2^T is generally very large and grows very rapidly with increasing $1/x$. The calculated curves for Ω_2^T from Fig. 4 confirm the experimental results that the AT splitting for a cascade scheme can

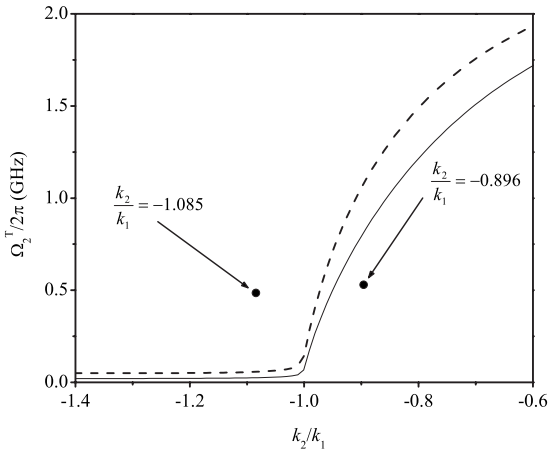

FIG. 4. The two lines represent the threshold coupling laser Rabi frequency ${\Omega_2}^T$ as a function of k_2/k_1 $(1/x)$. The solid line ${\Omega_2}^T$ is calculated using the parameters for experimental system A and the dashed line ${\Omega_2}^T$ is calculated with the parameters for experimental system B. The solid circles represent the coupling Rabi frequencies used in each experiment.

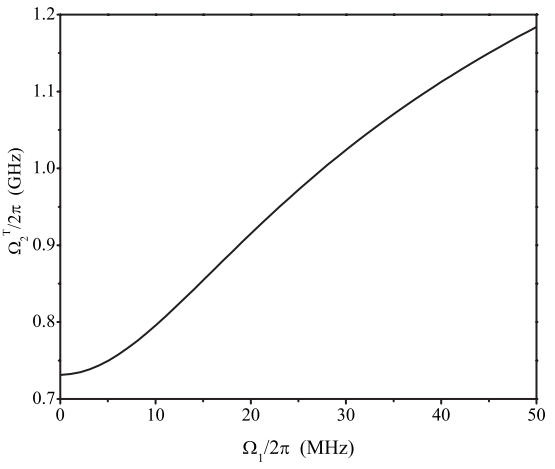

FIG. 5. Dependence of the threshold coupling laser Rabi frequency ${\Omega_2}^T$ as a function of the probe laser Rabi frequency Ω_1 calculated with the parameters for system B.

be observed relatively easily in Doppler-broadened samples only for counterpropagating laser beams when the probe laser wave number k_1 is smaller than the coupling laser wave number k_2, while in the case of counterpropagating beams, when the wave number of the probe laser k_1 is larger than the wave number of the coupling laser k_2, the splitting is very difficult to observe. The dependence of Ω_2^T on the wave-number ratio of the two lasers can be understood if we consider the dominant features in the expression for I_3 from Ref. [19],

$$I_3(\Delta_1,\Delta_2) \propto \frac{w(z_i)}{z_1 - z_2}, \tag{4}$$

where $w(z_i)$ is the Faddeeva function and z_1 and z_2 are the roots of the denominator of the perturbatively (small probe Rabi frequencies) derived expression for ρ_{33} from Refs. [14,19]. The term $1/(z_1-z_2)$ is the dominant one when $-1<x<0$ giving rise to the appearance of sharp narrow resonances for the AT effect in the recorded spectra at relatively small coupling Rabi frequencies. On the other hand, the term $w(z_k)$ gives rise to the appearance of a broad AT split line shape for any value of x but only at large enough coupling Rabi frequencies Ω_2.

The origin of the splitting due to the term $1/(z_1-z_2)$ and its dependence on x can be understood if we write it explicitly in terms of the probe laser detuning Δ_1,

$$\frac{1}{z_1 - z_2} \propto \frac{1}{[\Delta_1^2 - \Gamma^2 + x(x+1)\Omega_2^2]^2 + 4\Gamma^2\Delta_1^2}, \tag{5}$$

with $\Gamma = \gamma_{12}(1+x) - x\gamma_{13}$.

From the resonance condition of Eq. (5), $\Delta_1^2 - \Gamma^2 + x(x+1)\Omega_2^2 = 0$, and the fact that Γ is usually a small parameter, we see that

$$\Delta_1^{\text{AT splitting}} = 2\sqrt{-x(1+x)}\Omega_2 \quad \text{for} \quad -1 < x < 0, \tag{6}$$

where $\Delta_1^{\text{AT splitting}}$ is the peak-to-peak separation of the AT split spectra. The resonance condition in Eq. (5) exists only in the case $-1<x<0$, where the term $x(1+x)$ is negative, while when $x<-1$, the term $x(1+x)$ is positive and Eq. (5) has an extremum as a function of Δ_1 only at $\Delta_1=0$. At large enough coupling Rabi frequencies, the $w(z_i)$ terms become dominant and determine the AT splitting and shape of the spectra. If the argument of $w(z_i)$ satisfies $|z_i| \gg 1$ (fulfilled for $\Omega_2 \gg 1$), we have the asymptotic behavior $w(z_i) \sim (i/\sqrt{\pi})(1/z_i)$ [32]. As has been shown in Ref. [19], for this case for the AT splitting asymptotically we have

$$\Delta_1^{\text{AT splitting}} = \Omega_2. \tag{7}$$

Thus, the observed stark difference in AT splitting between systems A and B can be explained theoretically as the result of the interplay between the terms $1/(z_1-z_2)$ and $w(z_k)$ in Eq. (4). When $-1<x<0$, the first term is dominant and gives rise to AT split spectra at small to moderate Ω_2, while in the case of $x<-1$, only the second term can give rise to AT splitting which happens at large values of Ω_2.

IV. CONCLUSION

In conclusion, we have demonstrated experimental results that show profoundly different behavior of the AT splitting in the spectra from the upper level in a Doppler-broadened open molecular cascade system, while the EIT from the intermediate level is almost unaffected. We have shown that the reason for this unexpected behavior is the presence of Doppler broadening and that it is strongly dependent on the ratio of the probe and coupling laser wave numbers.

ACKNOWLEDGMENTS

This work was supported by National Science Foundation Grants No. PHY 0245311 and No. PHY 0555608. We gratefully acknowledge valuable discussions with Lorenzo M. Narducci of Drexel University and Frank C. Spano of Temple University.

[1] E. Arimondo, in *Progress in Optics XXXV*, edited by E. Wolf (Elsevier, Amsterdam, 1996).
[2] L. V. Hau, S. E Harris, Z. Dutton, and C. H. Behroozi, Nature **397**, 594 (1999).
[3] A. S. Zibrov, M. D. Lukin, L. Hollberg, D. E. Nikolov, M. O. Scully, H. G. Robinson, and V. L. Velichansky, Phys. Rev. Lett. **76**, 3935 (1996).
[4] S. E. Harris, Phys. Rev. Lett. **70**, 552 (1993).
[5] M. O. Scully and M. Fleischhauer, Phys. Rev. Lett. **69**, 1360 (1992).
[6] K.-J. Boller, A. Imamoglu, and S. E Harris, Phys. Rev. Lett. **66**, 2593 (1991).
[7] J. E. Field, K. H. Hahn, and S. E. Harris, Phys. Rev. Lett. **67**, 3062 (1991).
[8] D. J. Fulton, S. Shepherd, R. R. Moseley, B. D. Sinclair, and M. H. Dunn, Phys. Rev. A **52**, 2302 (1995).
[9] J. Gea-Banacloche, Y. Q. Li, S. Z. Jin, and M. Xiao, Phys. Rev. A **51**, 576 (1995).
[10] Y. Zhu, and T. N. Wasserlauf, Phys. Rev. A **54**, 3653 (1996).
[11] S. Baluschev, N. Leinfellner, E. A. Korsunsky, and L. Windholz, Eur. Phys. J. D **2**, 5 (1998).
[12] L. Sirko, A. Buchleitner, and H. Walther, Opt. Commun. **78**, 403 (1990).
[13] B. K. Teo, D. Feldbaum, T. Cubel, J. R. Guest, P. R. Berman, and G. Raithel, Phys. Rev. A **68**, 053407 (2003).
[14] J. Qi, F. C. Spano, T. Kirova, A. Lazoudis, J. Magnes, L. Li, L. M. Narducci, R. W. Field, and A. M. Lyyra, Phys. Rev. Lett. **88**, 173003 (2002).
[15] E. Ahmed, A. Hansson, P. Qi, T. Kirova, A. Lazoudis, S. Kotochigova, A. M. Lyyra, L. Li, J. Qi, and S. Magnier, J. Chem. Phys. **124**, 084308 (2006).
[16] J. Qi, G. Lazarov, X. Wang, L. Li, L. M. Narducci, A. M. Lyyra, and F. C. Spano, Phys. Rev. Lett. **83**, 288 (1999).
[17] R. Garcia-Fernandez, A. Ekers, J. Klavins, L. P. Yatsenko, N. N. Bezuglov, B. W. Shore, and K. Bergmann, Phys. Rev. A **71**, 023401 (2005).
[18] E. H. Ahmed, P. Qi, B. Beser, J. Bai, R. W. Field, J. P. Huennekens, and A. M. Lyyra, Phys. Rev. A **77**, 053414 (2008).
[19] E. Ahmed and A. M. Lyyra, Phys. Rev. A **76**, 053407 (2007).
[20] S. Magnier (private communication).
[21] T.-J. Whang, H. Wang, A. M. Lyyra, L. Li, and W. C. Stwalley, J. Mol. Spectrosc. **145**, 112 (1991).
[22] C.-C. Tsai, J. T. Bahns, H. Wang, T.-J. Wang, and W. C. Stwalley, J. Chem. Phys. **101**, 25 (1994).
[23] P. Qi, J. Bai, E. Ahmed, A. M. Lyyra, S. Kotochigova, A. J. Ross, C. Effantin, P. Zalicki, J. Vigue, G. Chawla, R. W. Field, T.-J. Whang, W. C. Stwalley, L. Li, and T. Bergeman, J. Chem. Phys. **127**, 044301 (2007).
[24] P. Kusch and M. M. Hessel, J. Chem. Phys. **68**, 2591 (1978).
[25] R. J. Le Roy, University of Waterloo Chemical Physics Research Report No. CP661, 2005.
[26] G. Baumgartner, H. Kornmeier, and W. Preuss, Chem. Phys. Lett. **107**, 13 (1984).
[27] A. Hansson and J. G. Watson, J. Mol. Spectrosc. **233**, 169 (2005).
[28] E. Tiemann, Z. Phys. D: At., Mol. Clusters **5**, 77 (1987).
[29] E. Tiemann, H. Knockel, and H. Richling, Z. Phys. D: At., Mol. Clusters **37**, 323 (1996).
[30] H. Richter, H. Knockel, and E. Tiemann, Chem. Phys. **157**, 217 (1991).
[31] J. Sagle, R. K. Namiotka, and J. Huennekens, J. Phys. B **29**, 2629 (1996).
[32] M. Abramowitz and I. A. Stegun, *Handbook of Mathematical Functions with Formulas Graphs and Mathematical Tables* (U. S. GPO, Washington, D.C., 1972).